Soil & Tillage Research 258 (2026) 107039

Contents lists available at ScienceDirect

Soil & Tillage Research

journal homepage: www.elsevier.com/locate/still

Conservation tillage could achieve SOC accumulation of eroding farmland in black soil regions

Rui Qian [a,b,c], Lei Gao [b,*], Wei Hu [d], Junjie Liu [a], Hao Du [b,c], Xinhua Peng [e,*]

[a] Key laboratory of Mollisols Agroecology, Northeast Institute of Geography and Agroecology, Chinese Academy of Sciences, Harbin 150081, China
[b] State Key Laboratory of Soil and Sustainable Agriculture, Institute of Soil Science, Chinese Academy of Sciences, Nanjing 211135, China
[c] University of Chinese Academy of Science, Beijing 100081, China
[d] New Zealand Institute for Bioeconomy Science Limited, Plant & Food Research Group, Private Bag 4704, Christchurch 8140, New Zealand
[e] State Key Laboratory of Efficient Utilization of Arable Land in China, Institute of Agricultural Resources and Regional Planning, Chinese Academy of Agricultural Sciences, Beijing 100081, China

ARTICLE INFO

Keywords:
Soil erosion
No-tillage
Straw mulch
Carbon mineralization
Carbon flux

ABSTRACT

Sloping farmland is highly vulnerable to soil organic carbon (SOC) depletion due to severe soil erosion. Conservation tillage has been widely promoted to enhance SOC storage, yet its effectiveness in reducing C loss and improving sequestration in these erosion-prone systems remains unclear. This study quantified SOC budget by assessing major C input and loss pathways under three tillage regimes: conventional tillage with straw removal (CT), conventional tillage with straw incorporation (CTS), and no-tillage with straw mulch (NTS), on a black soil hillslope of Northeast China. Results showed that CT induced a net soil C loss of −1016 kg C ha^{-1} yr^{-1}. Among all loss pathways, C mineralization was the dominant (>90 %), followed by sediment-associated transport (2.7 %–6.4 %). Relative to CT, CTS increased straw-derived C inputs and reduced sediment-associated losses, resulting in an 87.9 % decrease in net soil C loss. However, due to the substantial increase in C mineralization, it still resulted in net SOC depletion (-122 kg C ha^{-1} yr^{-1}). In contrast, NTS most effectively reduced both mineralization and sediment C loss, yielding a net soil C gain of 489 kg C ha^{-1} yr^{-1} . These results demonstrate that minimizing soil disturbance and retaining surface residues are essential for reducing C losses and enhancing SOC storage in erosion-prone sloping agroecosystems.

1. Introduction

Soil organic carbon (SOC) is fundamental to soil functioning, underpinning nutrient cycling, structural stability, and agricultural productivity (Johnson et al., 2024). Additionally, SOC mitigates rising atmospheric CO_2 concentrations by functioning as a major terrestrial C reservoir (Lal, 2004). However, this critical pool is highly susceptible to soil erosion, especially under intensive agricultural management. Indeed, soil erosion has emerged as a major driver influencing global SOC budget (Amundson et al., 2015).

Traditionally, erosion was viewed primarily as a mechanism of C loss (Jacinthe, Lal, 2001; Lal, 2003a, 2004). This perspective shifted when Harden et al. (1999) demonstrated that erosion can also promote SOC burial. To date, estimates of erosion-induced C fluxes remain highly uncertain, with reported values ranging from −1.2–1.5 Pg C yr^{-1} (Zheng et al., 2025). This debate largely reflects limited knowledge of SOC redistribution pathways and their spatial magnitudes across hillslopes (Wang et al., 2024). In erosion-affected landscapes, SOC depletion primarily occurs through two pathways: microbial mineralization and physical transport (Van Oost and Six, 2023). Vertical losses via mineralization are increasingly recognized as dominant, with studies estimating that more than half of the redistributed SOC may ultimately be mineralized to CO_2 (de Nijs and Cammeraat, 2020). Lateral transport through sediment-associated movement also constitutes a major loss pathway, typically resulting in SOC depletion in erosional zones and enrichment in depositional areas (Nie et al., 2016; Védère et al., 2022). In addition, dissolved organic carbon (DOC), the most labile SOC fraction, represents a transient pool mobilized both vertically through leaching and laterally via surface runoff (Gommet et al., 2022). However, DOC loss is often neglected in erosion studies due to its relatively small proportion of the total SOC pool (Yue et al., 2016), especially in the case of deep leaching, which remains difficult to quantify owing to

* Corresponding authors.
E-mail addresses: lgao@issas.ac.cn (L. Gao), pengxinhua@caas.cn (X. Peng).

https://doi.org/10.1016/j.still.2025.107039
Received 31 July 2025; Received in revised form 27 November 2025; Accepted 21 December 2025
Available online 26 December 2025

subsurface hydrological complexity (Doetterl et al., 2016; Wu et al., 2021). Therefore, a more comprehensive quantification of multiple C loss pathways and their relative contributions is critical for advancing our understanding of SOC fate in erosion-prone environments and refining regional C cycle models.

Tillage is a primary driver of erosion and SOC loss, particularly on sloping farmland during periods of intense rainfall (Peng et al., 2023). By disrupting soil structure and reducing surface protection, conventional tillage accelerates both C mineralization and physical export via runoff and sediment transport (Wang et al., 2017). In contrast, conservation tillage practices that minimize disturbance and retain crop residues have gained increasing attention for their effectiveness in reducing soil erosion in vulnerable agroecosystems (Madarász et al., 2021; Novara et al., 2021; Eskandari et al., 2022). For example, no-tillage with surface mulch in western Mexico substantially decreased sediment yield (Scopel et al., 2005), and a meta-analysis in China reported 36.1 % and 51.7 % reductions in runoff and sediment loss, respectively, under reduced-disturbance systems (Jia et al., 2019). While the erosion-mitigating benefits of conservation tillage are well established, its role in reducing SOC loss through multiple pathways on sloping farmland has not been comprehensively evaluated. To remedy this knowledge gap, it is critical to evaluate how tillage regimes regulate both vertical and lateral C fluxes in erosion-prone landscapes.

Northeast China, one of the world's major black soil regions, is a key grain-producing area. However, decades of intensive cultivation, coupled with rolling topography, concentrated summer rainfall, and widespread downslope ridge planting, have greatly intensified soil erosion and SOC loss in sloping farmlands (Ma et al., 2024). Since the launch of the Black Soil Conservation Program in 2020, conservation tillage has been widely promoted to restore soil quality and promote sustainable production. Although these practices have shown clear benefits for erosion control, their effectiveness in regulating C cycling in sloping agroecosystems remains unclear. This is partly due to the complexity of erosion-induced SOC processes, which are difficult to monitor under field conditions. As a result, most current studies rely heavily on model-based simulations with limited *in situ* validation, contributing to large uncertainties in quantifying erosion-related C fluxes. Therefore, *in situ* monitoring of C fluxes on eroded hillslopes is essential for clarifying C transport pathways, improving model calibration, and enhancing the accuracy of SOC budget assessments in erosion-prone regions.

This study examined the C budget through detailed *in situ* monitoring under three tillage practices on a typical hillslope in Northeast China: conventional tillage with straw removal (CT), conventional tillage with straw incorporation (CTS), and no-tillage with straw mulch (NTS). Carbon outputs were assessed through mineralization, sediment and runoff transport, and deep leaching, while inputs included root biomass and straw incorporation. We hypothesized that conservation tillage shifted soil C from net loss under conventional tillage to accumulation on sloping farmland. By monitoring the C budget across varied slope positions, this study aimed to elucidate the role of tillage practices in regulating soil C fluxes and sequestration in erosion-prone agricultural landscapes.

2. Materials and methods

2.1. Site description

The field experiment was conducted on a typical farming hillslope (47°23'03'' N, 126°50'39'' E) located in Hailun city, Heilongjiang Province, Northeast China. The region experiences a temperate continental monsoon climate, characterized by warm, humid summers and cold, dry winters. The mean annual temperature is approximately 1.5 °C, and annual precipitation ranges from 500 to 600 mm, with approximately 65 % occurring between June and August (China Meteorological Data Service Centre, 1961–2021). During the study period of 2023–2024, erosive rainfall varied markedly, with 481.2 mm in 2023 (76.6 % of annual precipitation) and 187 mm in 2024 (40.1 %) (Fig. 1).

The hillslope has been cultivated for over 60 years with around 15-cm tillage depth and straw removal. Maize and soybean are the main crops without irrigation. The undulating topography results in an elevation range from 213 to 235 m. The hillslope has experienced severe soil erosion, with averaged erosion rate of 4189.2 km^{-2} yr^{-1} in the past six decades (Qian et al., 2025). Prolonged erosion resulted in substantial differences in the thickness of the black soil layer, measuring 35 cm, 20 cm, and > 100 cm at the upper, middle, and lower positions, respectively. The soil is classified as Mollisol according to the USDA Soil Taxonomy. Soil properties of the top 15 cm were shown in Table 1, generally with relatively high clay and low nutrient contents.

2.2. Experiment design

To capture the SOC budget associated with erosion and deposition processes on sloping farmland, a whole-slope monitoring design was implemented that preserved natural hydrological connectivity from the slope crest to the toe (Fig. 2a). In October 2022, nine experimental plots were established on the hillslope (Fig. 2b). Each plot measured 360 m in length and 3.2 m in width and was laid out downslope to preserve natural hydrological connectivity. A randomized complete block design was employed, involving three tillage treatments: (i) conventional tillage with straw removal (CT), (ii) conventional tillage with straw incorporation (CTS), and (iii) no-tillage with straw mulch (NTS), each with three replicates. CT and CTS treatments involved moldboard plowing to a depth of approximately 15 cm each year before spring sowing.

The entire hillslope was divided into upper, middle, and lower zones according to distinct variations in slope gradient and the corresponding erosion rate (Fig. S1). The upper slope, extending from the summit to the point where the slope begins to steepen, has an average gradient of 3.2° and is subject to weak erosion. The middle slope represents the steepest section, with a mean gradient of 5.5° and strong erosion. The lower slope, extending from the point of gradient reduction to the toe, averages 2.2° and is characterized by deposition (Qian et al., 2025). Differences in soil profile properties further supported this zonation (Table S1). The strongly eroded middle slope exhibited the lowest surface nutrient levels and a rapid decline with depth, together with the highest clay fraction. In contrast, the lower slope showed higher nutrient contents and lower bulk density throughout the profile, consistent with its depositional characteristics.

Uniform crop management was adopted across all plots. A continuous maize cropping system was implemented during the study period.

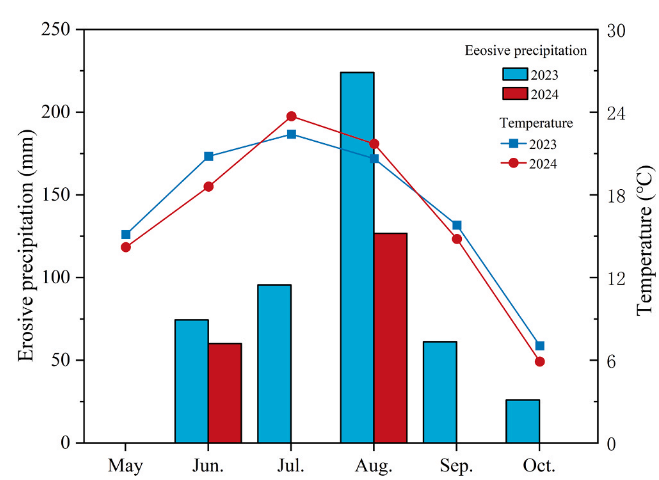

Fig. 1. Temporal dynamics of temperature and erosive rainfall of the study area between May and October in 2023–2024.

Table 1
Soil properties among tillage practices at lower, middle, and upper slope positions at 0–15 cm depth.

Properties	Treatments	Lower position	Middle position	Upper position
pH	CT	6.1 ± 0.06Bb	6.2 ± 0.06ABa	6.3 ± 0.1Aa
	CTS	6.3 ± 0.01Aa	6.4 ± 0.07Aa	6.4 ± 0.04Aa
	NTS	6.2 ± 0.07Aab	6.2 ± 0.1Aa	6.4 ± 0.06Aa
Bulk density (g cm^{-3})	CT	1.1 ± 0.07Ab	1.1 ± 0.04Ab	1.1 ± 0.02Ab
	CTS	1.1 ± 0.02Aab	1.1 ± 0.02Ab	1.1 ± 0.05Ab
	NTS	1.2 ± 0.02Aa	1.3 ± 0.01Aa	1.2 ± 0.02Aa
Sand content (%)	CT	9.9 ± 1.0Aa	9.4 ± 1.2Aa	7.3 ± 0.8Aa
	CTS	10.1 ± 1.1Aa	8.2 ± 0.5Aa	9.2 ± 0.9Aa
	NTS	8.3 ± 1.45Aa	6.2 ± 0.10Aa	8.5 ± 1.1Aa
Silt content (%)	CT	57.1 ± 1.3Aa	55.1 ± 2.9Aa	58.5 ± 1.2Aa
	CTS	54.5 ± 1.1Ba	52.7 ± 0.3Ba	58.9 ± 0.7Aa
	NTS	57.3 ± 0.5ABa	56.1 ± 1.5Ba	60.1 ± 0.6Aa
Clay content (%)	CT	33.0 ± 1.0Aa	35.5 ± 3.2Aa	34.2 ± 1.7Aa
	CTS	35.4 ± 1.2Ba	39.1 ± 0.4Ca	32.0 ± 0.4Aa
	NTS	34.4 ± 1.2Aa	37.7 ± 0.6Aa	31.5 ± 1.2Aa
Soil organic carbon (g kg^{-1})	CT	15.7 ± 0.7Ba	11.0 ± 1.7Ca	20.4 ± 0.4Aa
	CTS	15.8 ± 0.3Ba	10.8 ± 0.8Ca	20.1 ± 1.2Aa
	NTS	16.3 ± 0.8Aa	11.7 ± 1.6Ba	20.7 ± 1.1Aa
Total nitrogen (g kg^{-1})	CT	1.5 ± 0.4Ba	1.2 ± 0.4Ca	1.8 ± 0.2Aa
	CTS	1.5 ± 0.4Ba	1.1 ± 0.3Ca	1.7 ± 0.4Aa
	NTS	1.6 ± 0.2Aa	1.2 ± 0.8Ba	1.8 ± 0.3Aa

Note: Different lowercase letters indicate significant differences among tillage practices at the same position ($p < 0.05$). Different uppercase letters indicate significant differences among three positions for the same tillage practice ($p < 0.05$).

Each May, a no-till planter was used for seeding and fertilization. Spring maize (C1563) was sown at a rate of 22 kg ha^{-1} , with a row spacing of 65 cm and plant spacing of 20 cm. The crop was harvested in October. All treatments followed the local fertilization regime for maize cultivation on hillslopes, with each plot receiving a uniform rate of nitrogen (142 kg ha^{-1}), phosphate (62 kg ha^{-1}), and potassium (97 kg ha^{-1}), supplied through urea (46 % N) and a compound fertilizer ($N:P_2O_5:K_2O$ = 12:18:15).

2.3. *Carbon budgets monitoring*

Carbon budgets were monitored during the maize growing season, from the period following spring thaw (May) until to soil refreezing in late autumn (October). This period, with air temperatures typically above 0 °C, encompasses the majority of annual SOC mineralization. Concurrently, frequent and intense precipitation events often trigger surface runoff and soil detachment, leading to the translocation and loss of SOC. The monitored C pathways included mineralization, surface transport via runoff and sediment, and deep leaching losses.

2.3.1. *Carbon mineralization*

Carbon mineralization was assessed using a static closed chamber method coupled with gas chromatography. Static chambers were installed at the upper, middle, and lower positions within each plot (Fig. 2b). Each chamber consisted of a stainless-steel base frame (40 cm × 40 cm × 15 cm) inserted 15 cm into the soil, and a removable top box (40 cm × 40 cm × 30 cm). To eliminate interference from autotrophic respiration, maize plants and their roots were removed within a 1.5 m^2 area surrounding each chamber, and weeds were regularly removed throughout the monitoring period. Additionally, a fiber barrier was buried to a depth of 30 cm around each frame to prevent root intrusion. Whole-slope C mineralization was calculated as the area-weighted average of C mineralization from the upper, middle, and lower positions.

Gas sampling was conducted fortnightly throughout the growing season, and weekly during the initial phase of straw decomposition. Samples were collected at 10-minute intervals (0, 10, 20, and 30 min) between 9:00 and 12:00 (Jian et al., 2018). CO_2 concentrations were determined using a gas chromatograph (GC-2010, Shimadzu, Japan). The C mineralization rate (mg C m^{-2} h^{-1}) was calculated using the following equation:

$$F = \frac{dc}{dt} \bullet \frac{M}{V_0} \bullet \frac{P}{P_0} \bullet \frac{T}{T_0} \bullet H \quad (1)$$

where $\frac{dc}{dt}$ represents the rate of change in gas concentration (ppm h^{-1}), M is the gas molar mass (g mol^{-1}), P denotes local atmospheric pressure (Pa), V_0 is the molar volume at standard temperature and pressure (22.41 L mol^{-1}), P_0 and T_0 represent standard pressure (101,325 Pa) and temperature (273.15 K), T is the ambient temperature (K), and H is the chamber height (m). Given that the study primarily focuses on aerobic soil conditions, CH_4 emissions are negligible (less than 0.5 % of total C mineralization). Therefore, this research mainly uses CO_2 emissions to represent SOC mineralization.

2.3.2. *Erosion-transported C*

To monitor C loss through surface runoff and sediment transport, standard runoff collection systems were installed at the downslope end of each plot (Fig. 2b). Each system consisted of a primary tank (2.0 m × 1.0 m × 1.0 m) designed to capture all runoff and sediment from the plot. The tank was fitted with 13 evenly spaced circular overflow outlets (5 cm in diameter) to ensure uniform splitting of flow and sediment loads, with one outlet connected to a secondary tank (0.8 m^3) to collect overflow during extreme rainfall events.

Following each erosive rainfall event, the height of the water-sediment mixture in the tank was recorded, and the total mixture volume was calculated to estimate runoff. To avoid disturbance of settled sediments, a 50 mL surface water sample was first collected from each tank, filtered through a 0.45 μm membrane, and stored in polyethylene bottles for DOC analysis using a TOC analyzer (multi N/C 3100, Analytik Jena, Germany). The remaining water-sediment mixture in the tank were then thoroughly homogenized, and three 1 L sediment-water subsamples were collected with pre-weighed bottles in each tank. These subsamples were transported to the laboratory, weighed to calculate the density of the water-sediment mixture, air-dried, and reweighed to determine the dry sediment mass for sediment yield estimation. The dried sediments were then ground, sieved, and analyzed for SOC using the potassium dichromate volumetric method.

Runoff C loss (kg C ha^{-1}) was calculated using the following equation:

$$\text{Runoff C loss} = \frac{V}{A} \bullet DOC_{runoff} \bullet 10^{-6} \quad (2)$$

where V indicates the runoff volume (L), A is the runoff plot area (ha), and DOC_{runoff} is the DOC concentration (mg L^{-1}). Runoff volume was calculated using:

$$V = \frac{2.65 - \rho}{1.65} \bullet v \bullet H \bullet S \bullet 10^3 \quad (3)$$

where ρ denotes the density of the sediment-water mixture (g cm^{-3}), v is the sampling bottle volume (1 L), H is the mixture height in the tank (m),

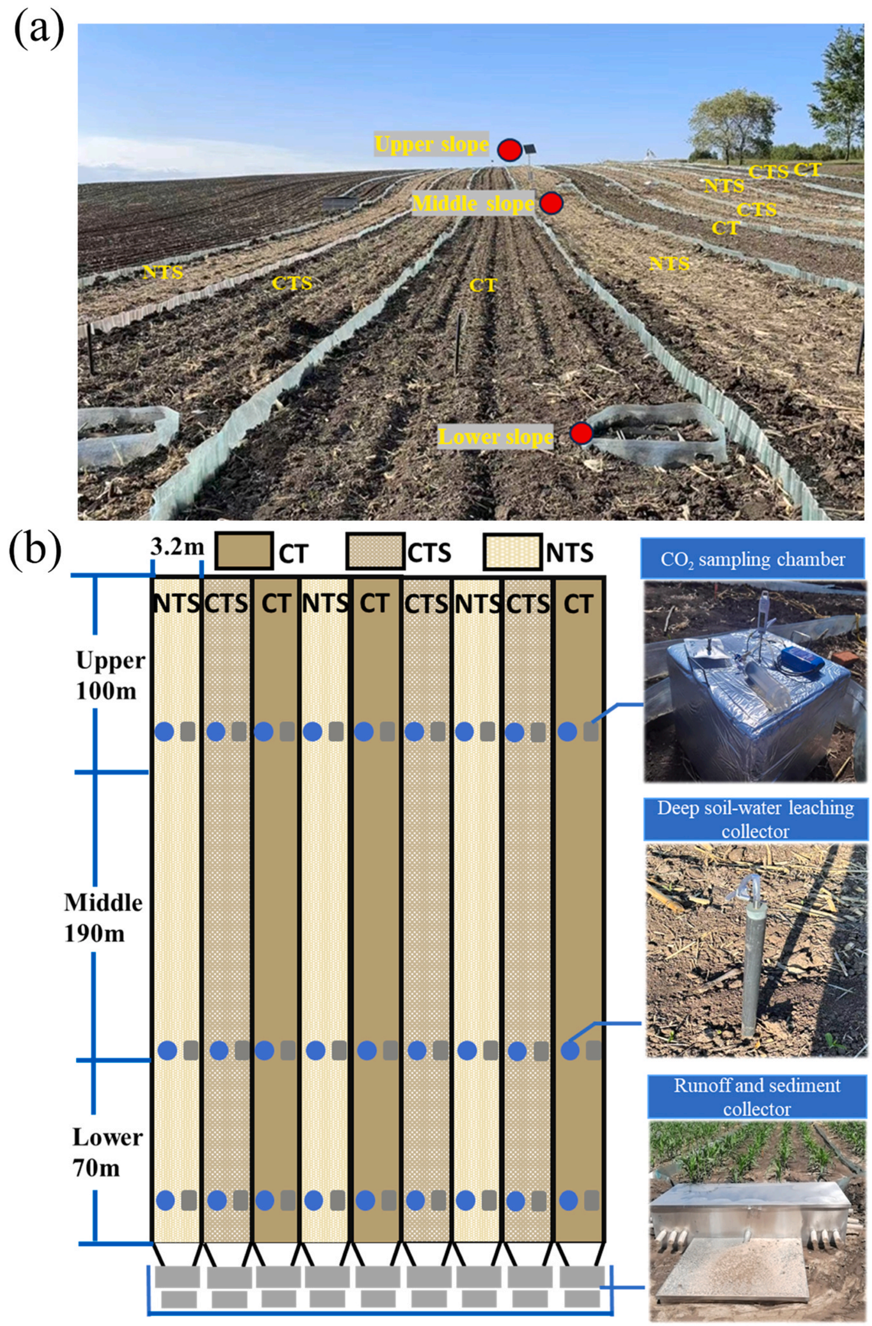

Fig. 2. Field view (a) and experimental plots layout (b) of the hillslope with different tillage practices. Grey squares indicate static chambers for CO_2 flux measurements, blue circles denote deep soil water collectors installed at 75 cm depth, and rectangular units at the plot outlets represent runoff and sediment collection tanks.

and S is the tank surface area (m^2). The value 2.65 represents average soil particle density (g cm^{-3}).

Sediment C loss (kg C ha^{-1}) was calculated as:

$$\text{Sediment C loss} = \frac{m \bullet H \bullet S}{A} \bullet SOC_{sediment} \bullet 10^{-3} \tag{4}$$

where m denotes the dry sediment mass per 1 L sample (g), and $SOC_{sediment}$ refers to the SOC content in sediment (g kg^{-1}).

2.3.3. Deep C leaching

Daily drainage at a soil depth of 100 cm was simulated for the upper, middle, and lower slope positions using the Hydrus-2D model (Šimůnek et al., 2005). The depth of 100 cm was chosen to represent deep drainage, as root activity is negligible at this depth and does not affect vertical DOC transport.

The water leaching flux was described by the Richards equation:

$$\frac{\partial \theta}{\partial t} = \frac{\partial}{\partial z}\left[K(h)\left(\frac{\partial h}{\partial z} + 1\right)\right] - s(z,\ t) \tag{5}$$

where θ denotes the volumetric water content (cm^3 cm^{-3}), t is time (d), z indicates soil depth (cm), $K(h)$ is the unsaturated hydraulic conductivity (cm d^{-1}), h is the soil water pressure head (cm), and $s(z,t)$ represents the root water uptake rate (cm d^{-1}). Soil hydraulic characteristics were described using the van Genuchten-Mualem model (Van Genuchten, 1980):

$$(h) = \begin{cases} \theta_r + \dfrac{\theta_s - \theta_r}{\left[1 + (\alpha h)^n\right]^m}, & h < 0 \\ \theta_s, & h \geq 0 \end{cases} \tag{6}$$

$$K(h) = K_s S_e^l \left[1 - \left(1 - S_e^{\frac{1}{m}}\right)^m\right]^2, \; S_e = \frac{\theta - \theta_r}{\theta_s - \theta_r} \tag{7}$$

where θ_s and θ_r represent the saturated and residual water content (cm^3 cm^{-3}), K_s denotes the saturated hydraulic conductivity (cm d^{-1}), m and n are empirical parameters, l is the pore connectivity factor, and S_e stands for effective saturation.

To evaluate the reliability of the simulated deep drainage at 100 cm, we compared simulated and measured soil water contents under the CT practice (Fig. S2; Du et al., 2024). The model reproduced hillslope soil water dynamics well ($R^2 = 0.81$; RMSE = 0.055 cm^3 cm^{-3}), supporting the credibility of the simulated deep drainage flux.

Soil pore water samplers (SK20, Eijkelkamp, Germany) were installed at 75 cm in each slope position to determine DOC concentration (Fig. 2b). Soil solution samples were collected twice monthly from May to October in 2023–2024, transferred to centrifuge tubes, stored at 4 °C, and analyzed using a TOC analyzer (multi N/C 3100, Analytik Jena, Germany).

Deep C leaching (kg C ha^{-1}) was calculated as:

$$\text{Deep C leaching} = D \times DOC_{leaching} \times 10^{-2} \tag{8}$$

where D is the simulated deep leaching flux at 100 cm and $DOC_{leaching}$ is the DOC concentration in soil solution (mg L^{-1}). Whole-slope deep C leaching was calculated as the area-weighted mean of losses from the three slope positions.

2.4. Biomass C input estimation

To estimate C input from crop residues, aboveground straw and root biomass were quantified at the upper, middle, and lower positions during the 2023–2024 maize harvest. In each position, representative plants were sampled from quadrats established in the central rows of each plot. Plants were divided at the brace root zone, with the portion above the brace roots (grain removed) classified as straw, and roots below excavated intact. Fresh weights were measured, samples were air-dried to determine dry biomass, and values were scaled to plant density to calculate biomass per unit area at each slope position. A C conversion coefficient of 0.45 was applied to estimate residue-derived C input (Kuzyakov, 2002). Whole-slope C input was obtained as the area-weighted average of the three slope positions.

2.5. Soil C flux calculation

Soil C flux (kg C ha^{-1}) on the hillslope from May to October was calculated using the following equation (Lugato et al., 2018; Liu, 2020):

$$C_{scf} = C_{input} - C_{output} \tag{9}$$

where C_{input} is the total C input (kg C ha^{-1}) and C_{output} is the total C loss (kg C ha^{-1}). These were determined as follows:

$$C_{input} = C_{st} + C_{rt} \tag{10}$$

$$C_{output} = C_{cm} + C_{rs} + C_{dl} \tag{11}$$

where C_{st} and C_{rt} represent C input from returned straw and root residues, respectively, and C_{cm}, C_{rs}, and C_{dl} denote C losses via cumulative mineralization, runoff and sediment transport, and deep leaching.

2.6. Soil sampling and analysis

Soil samples were collected in October 2024 from different slope positions and tillage treatments. For each plot, three soil cores were collected from 0 to 15 cm depth, yielding a total of 27 soil samples (three tillage practices × three slope positions × three replicates). Samples were cleared of roots, homogenized, sieved to 2 mm, and air-dried for laboratory analyses. Soil temperature and moisture were measured at 15 cm depth near the static chambers using a TDR 300 moisture meter (Spectrum, USA). Bulk density (BD) was determined using the core method. Soil pH was measured in a 1:2.5 soil: water suspension using a HI 3221 pH meter (Hanna Instruments Inc., USA). SOC was determined using the potassium dichromate oxidation method. Total nitrogen (TN) was measured using a CN analyzer (Vario Max CN, Germany).

2.7. Statistical analysis

Statistical analysis was performed using SPSS 20.0 software. One-way analysis of variance (ANOVA) was conducted to evaluate the effects of tillage practice on C budget. When significant differences were detected ($p < 0.05$), means were compared using the least significant difference test.

3. Results

3.1. Differences in C fluxes among tillage practices

Tillage practices significantly altered C loss pathways at the hillslope scale. Cumulative C mineralization over two growing seasons ranged from 1481.1 to 2796.3 kg C ha^{-1} among tillage practices (Fig. 3). Annually, CTS exhibited the highest cumulative mineralization, exceeding that of the CT and NTS by 81.5 % and 42.2 %, respectively ($p < 0.05$).

Physically transported C losses responded differently to tillage practices. Although CTS slightly reduced sediment-associated C loss compared with CT, it led to increased runoff-associated losses (Fig. 4a–b). In contrast, NTS significantly reduced both pathways relative to CT ($p < 0.05$), with sediment-associated losses reduced by 45.0 %, markedly more than the 38.4 % reduction in runoff C loss. Similar to runoff C loss, deep C leaching was also most pronounced under CTS, exceeding that under CT and NTS by 30.1 % and 17.5 %, respectively (Fig. 5; $p < 0.05$). Although NTS showed slightly higher deep leaching values than CT, the difference was not statistically significant. Between the two years, the lower frequency of erosive rainfall events in 2024 substantially reduced physical C transport compared to 2023.

Carbon inputs from maize straw and roots varied with tillage practice (Table 2). While CTS tended to produce greater straw-derived C

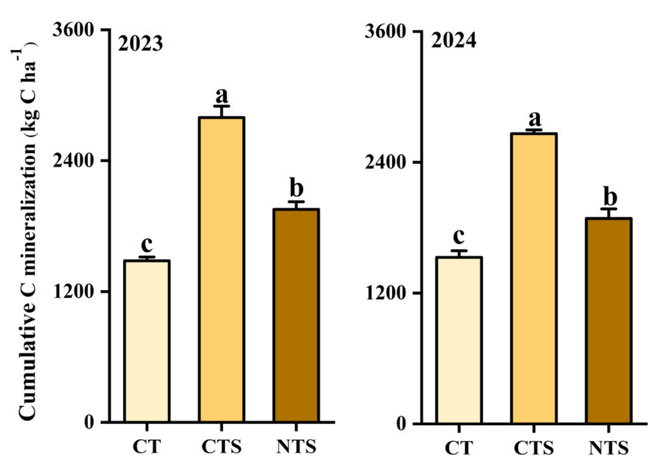

Fig. 3. Cumulative C mineralization of the hillslope under three tillage practices during 2023–2024. Different lowercase letters indicate significant differences among tillage practices ($p < 0.05$).

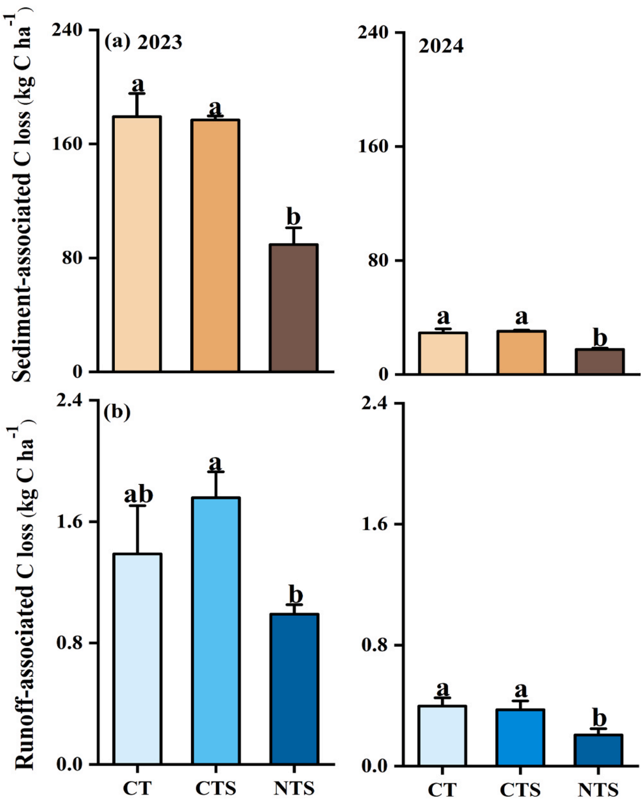

Fig. 4. Hillslope soil C losses in the forms of sediment transport (a) and surface runoff (b) under three tillage practices during 2023–2024. Different lowercase letters indicate significant differences among tillage practices ($p < 0.05$).

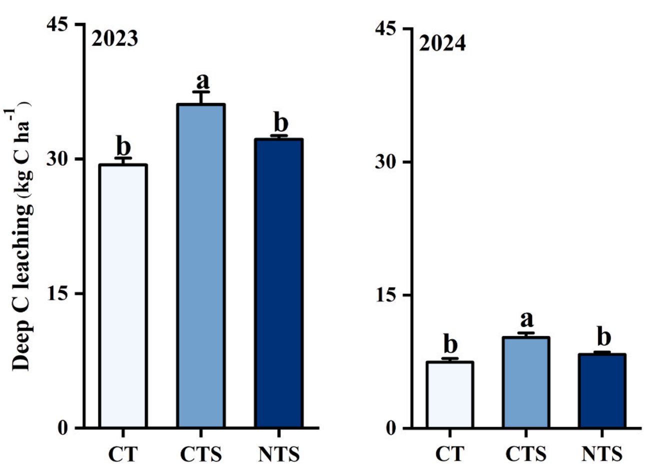

Fig. 5. Deep C leaching of the hillslope under three tillage practices during 2023–2024. Different lowercase letters indicate significant differences among tillage practices ($p < 0.05$).

Table 2
Annual C inputs from straw and root biomass under three tillage practices during 2023 and 2024.

C input sources	CT	CTS	NTS
Straw (kg C ha^{-1} yr^{-1})	NA	2043.5 ± 59.5a	1930.8 ± 12.5a
Root (kg C ha^{-1} yr^{-1})	612.1 ± 29.8b	691.8 ± 12.6a	557.3 ± 13.7b

Note: Different lowercase letters following the mean values ± standard deviation indicates significant differences among tillage practices ($p < 0.05$).

inputs than NTS, the difference was not significant. Root-derived C inputs followed the order CTS > CT > NTS, with values under CTS significantly exceeding those under CT and NTS by 13.0 % and 24.1 %, respectively ($p < 0.05$).

3.2. Soil C balance among tillage practices

Distinct tillage practices induced marked differences in annual soil C flux across the entire hillslope (Fig. 6). Although CTS reduced overall C losses by 87.9 % compared to CT ($p < 0.05$), it still resulted in net C depletion (-122 kg C ha^{-1} yr^{-1}), primarily due to increased mineralization. In contrast, NTS reversed this pattern, yielding a net gain of 489 kg C ha^{-1} yr^{-1} , which was 1505 kg ha^{-1} yr^{-1} higher than CT. This corresponded to an annual SOC increase of approximately 0.8 g kg^{-1} in the 0–15 cm soil layer, consistent with the observed ~0.7 g kg^{-1} (5 %) increase in SOC under NTS relative to CT in 2024 (Table 1).

Among all C loss pathways, mineralization was the dominant contributor, accounting for over 90 % of total C loss, followed by sediment-associated transport, which represented 2.7–6.4 %. Losses via deep leaching and surface runoff were minimal, contributing less than 2 % annually.

4. Discussion

4.1. Dominant pathways of hillslope C loss

Our results demonstrated that C mineralization dominated total C loss along the hillslope (Fig. 6), in agreement with earlier findings that over 50 % of erosion-induced SOC is released through mineralization, making erosion a significant source of atmospheric CO_2 (Jacinthe et al., 2002; Wang et al., 2014). This dominance can be attributed to the continuous nature of microbially mediated C mineralization, in contrast to physical C losses via erosion, which are episodic and confined to rainfall events (Fig. 1). The cumulative impact of sustained microbial activity therefore exceeds that of intermittently occurring sediment and runoff losses. These findings indicate that C loss in sloping farmland is governed not only by the magnitude of physical erosion but also by the strong influence of biological decomposition processes. Nevertheless, it should be noted that mineralization was monitored during the period from May to October. While this period captures the major phase of microbial activity, the reported values likely underestimate total annual mineralization.

Given the predominant role of C mineralization in regulating soil C fluxes, its substantial variation among tillage practices has critical implications for C balance. Results showed that CTS practice exhibited the highest accumulative C mineralization (Fig. 3). This enhancement primarily stems from the combined effects of added labile C from straw incorporation and tillage-induced soil disturbance, which collectively stimulate microbial activity. Tillage disrupts soil aggregate structure, exposing previously protected C while improving soil aeration, thereby promoting microbial proliferation and accelerating decomposition (Han et al., 2024). Furthermore, CTS provides more abundant substrates that facilitate the formation of more complex microbial network structures, exhibiting higher metabolic activity and functional diversity that further enhance C mineralization (Chen et al., 2023). In contrast, NTS treatment maintains aggregate integrity due to the absence of mechanical disturbance, thereby limiting microbial access to C pools (Li et al., 2024). Additionally, the higher soil moisture and reduced aeration under NTS (Fig. S3) may further suppress microbial respiration, resulting in lower C mineralization compared to CTS.

4.2. The role of soil erosion in C balance

Although sediment-associated C accounted for less than 10 % of total C loss at the slope scale (Fig. 6), its local impact may be underestimated. Substantial sediment deposition at the lower position likely obscured the

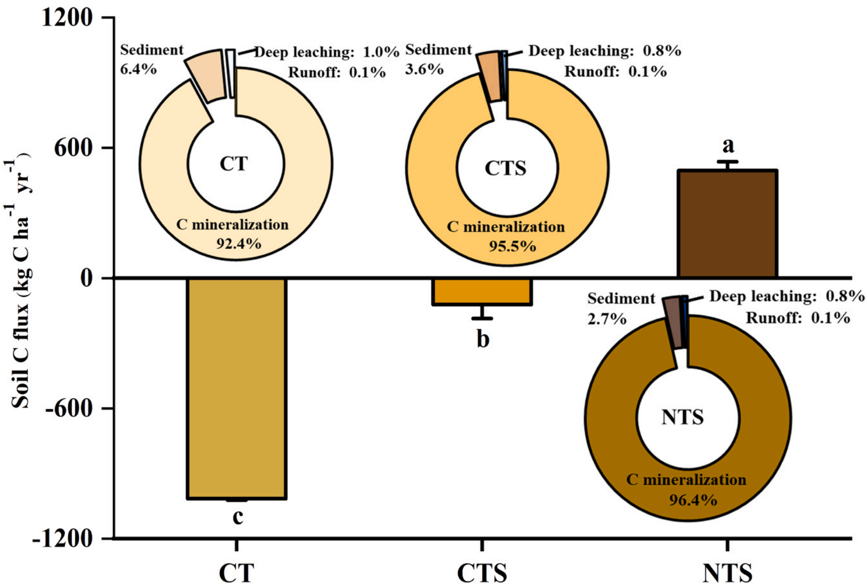

Fig. 6. Carbon balance status for 2023–2024 and the relative contributions of carbon loss pathways under three tillage practices. Different lowercase letters indicate significant differences among tillage practices ($p < 0.05$).

pronounced C depletion occurring in the mid-slope erosion zone. Previous studies indicate that erosion induces complex spatial redistribution of SOC in sloping croplands (Van Oost et al., 2007). In erosion zones, surface soils exhibit lower bulk density and looser structure due to higher SOC content (Lal, 2022), making surface C more susceptible to preferential removal by runoff. This persistent SOC translocation not only directly diminishes C storage capacity in erosion zones but also facilitates the transfer and redeposition of mobilized SOC downslope. Evidence suggests that over 50 % of eroded SOC can accumulate in depositional zones, forming important secondary C sinks (Panagos et al., 2015; Dialynas et al., 2016). This redistribution pattern is corroborated by our profile data: Mid-slope positions show consistently low SOC levels throughout the soil profile (Fig. S4), reflecting long-term surface soil stripping and C depletion. In contrast, the lower positions demonstrate a significant SOC increase with depth, reaching 20 g kg^{-1} below 1 m depth, indicating deep C enrichment through continuous deposition.

These findings emphasize that although sediment C loss represents a relatively small proportion of total C loss, its role in slope-scale SOC redistribution should not be overlooked. Given the unquantified sediment-associated C fluxes across different slope positions in this study, position-specific monitoring should be prioritized in future

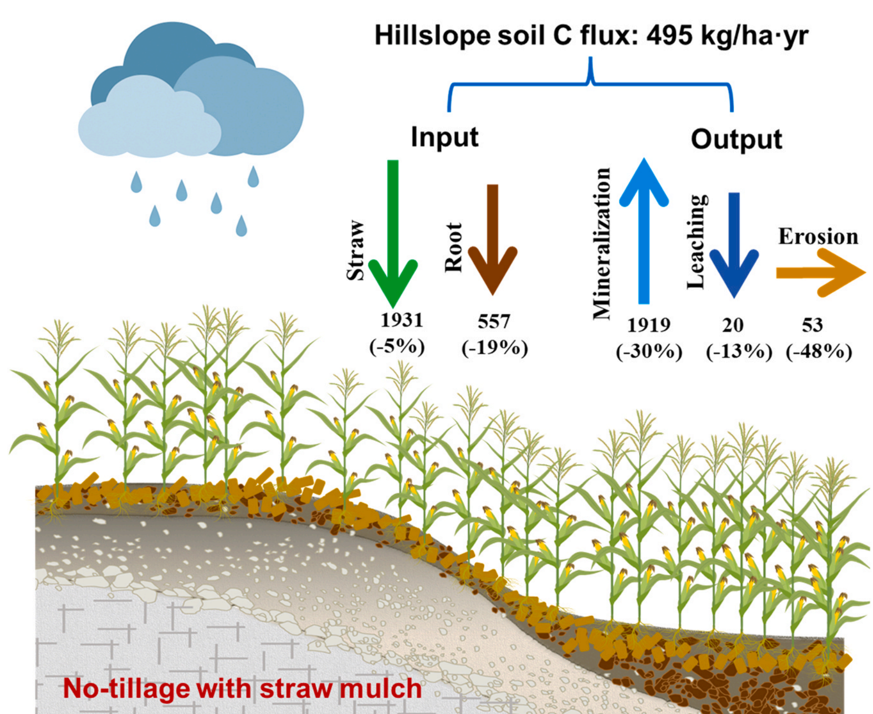

Fig. 7. Conceptual diagrams of soil C flux under NTS practice at hillslope scale. The percentages in parentheses represent the relative change for each C flux component relative to CTS practice.

studies to better elucidate SOC budget under erosion-deposition processes.

4.3. Conservation tillage enhances soil C storage of agricultural hillslopes

Our study confirmed that conventional tillage induced net soil C loss in sloping farmland, whereas conservation tillage effectively reversed this trend, annually increasing SOC stocks in the 0–15 cm layer by approximately 5 % relative to conventional tillage (Table 1, Fig. 6, and Fig. 7). These findings align with a meta-analysis by He et al. (2022) in Northeast China, which reported an average 8.1 % increase in surface SOC under conservation tillage relative to CT. The C accumulation observed under NTS has been widely reported to depend on sustained C inputs, reduced microbial decomposition, and suppressed physical C loss (Doetterl et al., 2016). However, NTS exhibited differential regulation of various physical C loss pathways in our study: it significantly reduced sediment-associated C loss but showed inconsistent effects on DOC transport (Fig. 4, Fig. 5). Mechanistically, surface residue retention under NTS dissipates raindrop kinetic energy, reduces overland flow velocity, and improves aggregate stability through eliminating tillage disturbance (Maetens et al., 2012; Wang et al., 2022), collectively limiting sediment-associated C mobilization. Conversely, although NTS elevated DOC concentrations and thereby promoted greater leaching compared with CT, it simultaneously decreased runoff-induced transport, implying spatial redistribution rather than an overall rise in DOC export.

Despite involving crop residues, CTS and NTS exerted contrasting effects on soil C budget. CTS exhibited a negative soil C flux (Fig. 6), primarily because tillage-stimulated microbial activity accelerates C mineralization. This divergence underscores that in erosion-prone soils, C input alone is insufficient for conservation; it must be coupled with physical protection mechanisms to maximize sequestration. Notably, although NTS showed the greatest SOC sequestration potential, it did not enhance maize yields during this two-year study, performing even worse than CT and CTS (Fig. S5). The yield response to conservation tillage in Northeast China's black soil region displays significant spatial variability. Previous studies indicate that no-till systems typically underperform conventional tillage in colder regions (He et al., 2022), whereas their yield advantages emerge as temperatures increase (Verhulst et al., 2011; Kan et al., 2020). Thus, our study region's low temperatures may partially explain the yield limitation. Additionally, no-till-induced surface compaction could restrict early crop growth and root development, further constraining yield potential (Van Ittersum, 2016; Wang et al., 2019; Qian et al., 2025). In summary, while NTS enhanced SOC storage, its agronomic benefits were not evident within the two-year study period. Given the multifactorial nature of yield responses, the long-term impacts of conservation tillage practices require continued monitoring to fully assess trade-offs between C sequestration and crop production.

5. Conclusions

This study systematically evaluated C budget under three tillage practices in sloping farmland of China's black soil region. The results demonstrate that conventional tillage induced net SOC loss, primarily attributable to C mineralization followed by sediment-associated C export. Among all tillage systems, conservation tillage proved most effective in enhancing SOC storage in erosion-prone landscapes, significantly reducing both C mineralization and sediment C losses. Given the extensive distribution of sloping farmland in the black soil region and their increasing vulnerability to soil degradation, these findings provide a scientific basis for formulating region-specific management strategies that promote long-term SOC sequestration.

While the study hillslope represents typical conditions of the black soil region, these findings are derived from a two-year experiment at a single site under specific soil and climatic conditions. Long-term uncertainties remain, including whether the SOC sequestration efficiency of conservation tillage declines with continued implementation and how the potential trade-off between C sequestration and crop yield evolves over time. Future research should involve long-term and multi-site trials across different agroecological zones to capture cumulative effects, assess the persistence of conservation tillage benefits, and clarify the long-term balance between soil C gains and agricultural productivity.

CRediT authorship contribution statement

Lei Gao: Writing – review & editing, Supervision, Funding acquisition. **Rui Qian:** Writing – review & editing, Writing – original draft, Formal analysis. **Junjie Liu:** Writing – review & editing. **Wei Hu:** Writing – review & editing. **Xinhua Peng:** Writing – review & editing, Supervision, Funding acquisition. **Hao Du:** Methodology.

Declaration of Competing Interest

The authors declare that they have no known competing financial interests or personal relationships that could have appeared to influence the work reported in this paper.

Acknowledgments

This work was financially supported by the Strategic Priority Research Program of the Chinese Academy of Sciences (XDA28010101, XDA28010403).

Appendix A. Supporting information

Supplementary data associated with this article can be found in the online version at doi:10.1016/j.still.2025.107039.

Data availability

Data will be made available on request.

References

Amundson, R., Berhe, A.A., Hopmans, J.W., Olson, C., Sztein, A.E., Sparks, D.L., 2015. Soil and human security in the 21 st century. Science 48 (6235), 1261071–1261076. https://doi.org/10.1126/SCIENCE.1261071.

Chen, X., Han, X.Z., Wang, X.H., Guo, Z.X., Yan, J., Lu, X.C., Zou, W.X., 2023. Inversion tillage with straw incorporation affects the patterns of soil microbial co-occurrence and multi-nutrient cycling in a Hapli-Udic Cambisol. Integr. Agric. 22 (5), 1546–1559. https://doi.org/10.1016/j.jia.2022.12.011.

China Meteorological Data Service Centre, 2021. Meteorological dataset for Northeast China. China Meteorological Administration, pp. 1961–2021. ⟨http://data.cma.cn⟩ (Available at).

Dialynas, Y.G., Bastola, S., Bras, R.L., Marin-Spiotta, E., Silver, W.L., Arnone, E., Noto, L. V., Richter, D., de, B., 2016. Impact of hydrologically driven hillslope erosion and landslide occurrence on soil organic carbon dynamics in tropical watersheds. Water Resour. Res. 52 (11), 8895–8919. https://doi.org/10.1002/2016WR018925.

Doetterl, S., Berhe, A.A., Nadeu, E., Wang, Z., Sommer, M., Fiener, P., 2016. Erosion, deposition and soil carbon: a review of process-level controls, experimental tools and models to address C cycling in dynamic landscapes. EarthSci. Rev. 154, 102–122. https://doi.org/10.1016/j.earscirev.2015.12.005.

Du, H., Gao, L., Qian, R., Wang, Y.J., Wang, J.X., Peng, X.H., 2024. Vertical migration flux of soil carbon and nitrogen of sloping farmland in typical black soil areas. Bull. Mineral. Petrol. Geochem 44 (04), 710–719. https://doi.org/10.3724/j.issn.1007-2802.20240118.

Eskandari, D.H., Khosravi, H., Habashi, K., Eskandari, D.H., Tiefenbacher, J.P., 2022. The impact of land use and land cover changes on soil erosion in western Iran. Nat. Hazards 1–21. https://doi.org/10.1007/s11069-021-05032-w.

Gommet, C., Lauerwald, R., Ciais, P., Guenet, B., Zhang, H., Regnier, P., 2022. Spatiotemporal patterns and drivers of terrestrial dissolved organic carbon (DOC) leaching into the European river network. Earth Syst. Dyn. 13 (1), 393–418. https://doi.org/10.5194/esd-13-393-2022.

Han, C., Zhou, W., Gu, Y., Wang, J., Zhou, Y., Xue, Y., Shi, Z., Siddique, K.H., 2024. Effects of tillage regime on soil aggregate-associated carbon, enzyme activity, and microbial community structure in a semiarid agroecosystem. Plant Soil 498 (1), 543–559. https://doi.org/10.1007/s11104-023-06453-1.

Harden, J.W., Sharpe, J.M., Parton, W.J., Ojima, D.S., Fries, T.L., Huntington, T.G., Dabney, S.M., 1999. Dynamic replacement and loss of soil carbon on eroding cropland. Glob. Biogeochem. Cycles 13, 885–901. https://doi.org/10.1029/1999GB900061.

He, C., Niu, J.R., Xu, C.T., Han, S.W., Bai, W., Song, Q.L., Dang, Y.P., Zhang, H.L., 2022. Effect of conservation tillage on crop yield and soil organic carbon in Northeast China: a meta-analysis. Soil Use Manag. 38 (2), 1146–1161. https://doi.org/10.1111/sum.12784.

Jacinthe, P.A., Lal, R., Kimble, J.M., 2002. Carbon dioxide evolution in runoff from simulated rainfall on long-term no-till and plowed soils in southwestern Ohio. Soil Tillage Res 66 (1), 23–33. https://doi.org/10.1016/S0167-1987(02)00010-7.

Jacinthe, P.A., Lal, R., 2001. A mass balance approach to assess carbon dioxide evolution during erosional events. Land Degrad. Dev. 12, 329–339. https://doi.org/10.1002/ldr.454.

Jia, L., Zhao, W., Fu, B., Daryanto, S., Wang, S., Liu, Y., Zhai, R., 2019. Effects of minimum soil disturbance practices on controlling water erosion in China's slope farmland: a meta-analysis. Land Degrad. Dev. 30 (6), 706–716. https://doi.org/10.1002/ldr.3258.

Jian, J., Steele, M.K., Day, S.D., Thomas, R.Q., Hodges, S.C., 2018. Measurement strategies to account for soil respiration temporal heterogeneity across diverse regions. Soil Biol. Biochem 125, 167–177. https://doi.org/10.1016/j.soilbio.2018.07.003.

Johnson, K., Kihara, J., Fan, M., Congreves, K.A., González-Pérez, J.A., Deb, S., de Vries, F., 2024. Understanding soil health. One Earth 7 (12), 2088–2091. https://doi.org/10.1016/j.oneear.2024.11.011.

Kan, Z.R., Liu, Q.Y., He, C., Jing, Z.H., Virk, A.L., Qi, J.Y., Zhao, X., Zhang, H.L., 2020. Responses of grain yield and water use efficiency of winter wheat to tillage in the North China Plain. Field Crop Res 249, 107760. https://doi.org/10.1016/j.fcr.2020.107760.

Kuzyakov, Y., 2002. Separating microbial respiration of exudates from root respiration in non-sterile soils: a comparison of four methods. Soil Biol. Biochem 34 (11), 1621–1631. https://doi.org/10.1016/S0038-0717(02)00146-3.

Lal, R., 2003a. Soil erosion and the global carbon budget. Environ. Int. 29, 437–450. https://doi.org/10.1016/S0160-4120(02)00192-7.

Lal, R., 2004. Soil carbon sequestration impacts on global climate change and food security. Science 304, 1623–1627. https://doi.org/10.1126/science.1097396.

Lal, R., 2022. Fate of soil carbon transported by erosional processes. Appl. Sci. 12 (1), 48. https://doi.org/10.3390/app12010048.

Li, M., Li, X., Shi, Y., Jiang, Y., Xue, R., Zhang, Q., 2024. Soil enzyme activity mediated organic carbon mineralization due to soil erosion in long gentle sloping farmland in the black soil region. Sci. Total Environ. 929, 172417. https://doi.org/10.1016/j.scitotenv.2024.172417.

Liu, P.Q., 2020. Organic Carbon Balance And Influencing Factors Under Different Tillage Practices In Flat And Sloping Black Soil Farmland of Northeast China. Master's thesis. Chinese Academy of Agricultural Sciences. https://doi.org/10.27630/d.cnki.gznky.2020.000825.

Lugato, E., Smith, P., Borrelli, P., Panagos, P., Ballabio, C., Orgiazzi, A., Fernandez-Ugalde, O., Montanarella, L., Jones, A., 2018. Soil erosion is unlikely to drive a future carbon sink in Europe. Sci. Adv. 4, eaau3523. https://doi.org/10.1126/sciadv.aau3523.

Ma, R., Tian, Z., Zhao, Y., Wu, Y., Liang, Y., 2024. Response of soil quality degradation to cultivation and soil erosion: a case study in a Mollisol region of Northeast China. Soil Tillage Res 242, 106159. https://doi.org/10.1016/j.still.2024.106159.

Madarász, B., Jakab, G., Szalai, Z., Juhos, K., Kotroczó, Z., Tóth, A., Ladányi, M., 2021. Long-term effects of conservation tillage on soil erosion in Central Europe: a random forest-based approach. Soil Till. Res. 209, 104959. https://doi.org/10.1016/j.still.2021.104959.

Maetens, W., Poesen, J., Vanmaercke, M., 2012. How effective are soil conservation techniques in reducing plot runoff and soil loss in Europe and the Mediterranean? Earth Sci. Rev. 115, 21–36. https://doi.org/10.1016/j.earscirev.2012.08.003.

Nie, X.J., Zhang, J.H., Cheng, J.X., Gao, H., Guan, Z.M., 2016. Effect of soil redistribution on various organic carbons in a water and tillage-eroded soil. Soil Till. Res. 155, 1–8. https://doi.org/10.1016/j.still.2015.07.003.

de Nijs, E.A., Cammeraat, E.L., 2020. The stability and fate of Soil Organic Carbon during the transport phase of soil erosion. Earth Sci. Rev. 201, 103067. https://doi.org/10.1016/j.earscirev.2019.103067.

Novara, A., Sarno, M., Gristina, L., 2021. No till soil organic carbon sequestration could be overestimated when slope effect is not considered. Sci. Total Environ. 757, 143758. https://doi.org/10.1016/j.scitotenv.2020.143758.

Panagos, P., Borrelli, P., Poesen, J., Ballabio, C., Lugato, E., Meusburger, K., Montanarella, L., Alewell, C., 2015. The new assessment of soil loss by water erosion in Europe. Environ. Sci. Policy 54, 438–447. https://doi.org/10.1016/j.envsci.2015.08.012.

Peng, Q., Liu, B., Hu, Y., Wang, A., Guo, Q., Yin, B., Yang, D., Zhang, K., Zhao, Y., He, L., 2023. The role of conventional tillage in agricultural soil erosion. Agric. Ecosyst. Environ. 348, 108407. https://doi.org/10.1016/j.agee.2023.108407.

Qian, R., Gao, L., Biswas, A., Du, H., Liu, S., Peng, X.H., 2025. Decoupling erosion effects on carbon fractions and stability in black soil agricultural landscapes. Pedosphere. https://doi.org/10.1016/j.pedsph.2025.09.024.

Qian, Y., Zhang, Z., Jiang, F., Wang, J., Dong, F., Liu, J., Peng, X., 2025. Impacts of tillage treatments on soil physical properties and maize growth at two sites under different climatic conditions in black soil region of Northeast China. Soil Till. Res., 106471 https://doi.org/10.1016/j.still.2025.106471.

Scopel, E., Findeling, A., Guerra, E.C., Corbeels, M., 2005. Impact of direct sowing mulch-based crop systems on soil carbon soil erosion and maize yield. Agron. Sustain. Dev. 25 (4), 425–432. https://doi.org/10.1051/agro:2005041.

Šimůnek, J., van Genuchten, M.T., Šejna, M., 2005. The HYDRUS-1D software package for simulating the one-dimensional movement of water heat and multiple solutes in variably-saturated media. Univ. Calif. Riverside Res. Rep. 3, 1–240.

Van Genuchten, M.T., 1980. A closed-form equation for predicting the hydraulic conductivity of unsaturated soils. Soil Sci. Soc. Am. J. 44 (5), 892–898. https://doi.org/10.2136/sssaj1980.03615995004400050002x.

Van Ittersum, M.K., 2016. Crop yields and global food security: will yield increase continue to feed the world? Eur. Rev. Agric. Econ. 43, 191–192. https://doi.org/10.1093/erae/jbv002.

Van Oost, K., Quine, T.A., Govers, G., De Gryze, S., Six, J., Harden, J.W., Ritchie, J.C., McCarty, G., W., Heckrath, G., Kosmas, C., Giraldez, J.V., Marques da Silva, J.R., Merckx, R., 2007. The impact of agricultural soil erosion on the global carbon cycle. Science 318, 626–629. https://doi.org/10.1126/science.1145724.

Van Oost, K., Six, J., 2023. Reconciling the paradox of soil organic carbon erosion by water. Biogeosciences 20 (3), 635–646. https://doi.org/10.5194/bg-20-635-2023.

Védère, C., Lebrun, M., Honvault, N., Aubertin, M.L., Girardin, C., Garnier, P., Dignac, M. F., Houben, D., Rumpel, C., 2022. How does soil water status influence the fate of soil organic matter? A review of processes across scales. Earth Sci. Rev. 234, 104214. https://doi.org/10.1016/j.earscirev.2022.104214.

Verhulst, N., Nelissen, V., Jespers, N., Haven, H., Sayre, K.D., Raes, D., Deckers, J., Govaerts, B., 2011. Soil water content, maize yield and its stability as affected by tillage and crop residue management in rainfed semi-arid highlands. Plant Soil 344, 73–85. https://doi.org/10.1007/s11104-011-0728-8.

Wang, X., Cammeraat, E.L., Romeijn, P., Kalbitz, K., 2014. Soil organic carbon redistribution by water erosion – the role of CO_2 emissions for the carbon budget. PLoS One 9 (5), e96299. https://doi.org/10.1371/journal.pone.0096299.

Wang, L., Dalabay, N., Lu, P., Wu, F., 2017. Effects of tillage practices and slope on runoff and erosion of soil from the Loess Plateau, China, subjected to simulated rainfall. Soil Till. Res. 166, 147–156. https://doi.org/10.1016/j.still.2016.09.007.

Wang, X., Fan, J., Xing, Y., Xu, G., Wang, H., Deng, J., Wang, Y., Zhang, F., Li, P., Li, Z., 2019. The effects of mulch and nitrogen fertilizer on the soil environment of crop plants. Adv. Agron. 153, 121–173. https://doi.org/10.1016/bs.agron.2018.08.002.

Wang, L., Nie, X., Li, J., Liu, Y., Wang, H., Li, Y., Li, Z., 2024. Erosion-induced recovery CO_2 sink offset the horizontal soil organic carbon removal at the basin scale. Sci. China Earth Sci. 67 (6), 2019–2033. https://doi.org/10.1007/s11430-023-1275-2.

Wang, L., Yen, H., Huang, C.H., Wang, Y., 2022. Erosion and covered zones altered by surface coverage effects on soil nitrogen and carbon loss from an agricultural slope under laboratory-simulated rainfall events. Int. Soil Water Conserv. Res. 10 (3), 382–392. https://doi.org/10.1016/j.iswcr.2022.01.002.

Wu, Q., Liang, H., Xiong, K., Li, R., 2021. Effectiveness of monitoring methods for soil leakage loss in karst regions. Environ. Earth Sci. 80 (7), 1–13. https://doi.org/10.1007/s12665-021-09593-8.

Yue, Y., Ni, J., Ciais, P., Piao, S., Wang, T., Huang, M., Borthwick, A.G., Li, T., Wang, Y., Chappell, A., Van Oost, K., 2016. Lateral transport of soil carbon and land−atmosphere CO_2 flux induced by water erosion in China. Proc. Natl. Acad. Sci. 113 (24), 6617–6622. https://doi.org/10.1073/pnas.1523358113.

Zheng, H., Miao, C., Huntingford, C., Tarolli, P., Li, D., Panagos, P., Yue, Y., Borrelli, P., Van Oost, K., 2025. The impacts of erosion on the carbon cycle. e2023RG000829 Rev. Geophys 63 (1). https://doi.org/10.1029/2023RG000829.